JOINT BLIND DECONVOLUTION AND SPECTRAL UNMIXING OF HYPERSPECTRAL IMAGES

Qiang Zhang
Dept. of Biostatistical Sciences, Wake Forest University, Winston-Salem, NC 27109

V. Paúl Pauca
Dept. of Computer Science, Wake Forest University, Winston-Salem, NC 27109

Robert Plemmons
Dept. of Mathematics and Computer Science, Wake Forest University, Winston-Salem, NC 27109

Our interest here is spectral imaging for space object identification based upon imaging using simultaneous measurements at different wavelengths. AMOS sensors can collect simultaneous images ranging from visible to LWIR. Multiframe blind deconvolution (MFBD) has demonstrated success by acquiring near-simultaneous multiple images for reconstructing space objects, and another success has been shown through adding phase diversity (PD) by splitting the light beam in channels with different phase functions. So far, most MFBD and PD applications have been focused on monochromatic images, with a few MFBD studies on multispectral images, also called the wavelength diversity. In particular, B. Calef has shown that wavelength-diverse MFBD is a promising technique for combining data from multiple sensors to yield a higher-quality reconstructed image. Here, we present optimization algorithms to blindly deconvolve observed blurred and noisy hyperspectral images with phase diversity at each wavelength channel. We use the facts that at longer wavelengths, turbulence effects on the phase are less severe, while diffraction effects at shorter wavelengths are less severe. Moreover, because the blurring kernels of all wavelength channels essentially share the same optimal path difference (OPD) function, we have greatly reduced the number of parameters in the blurring kernel. We model the true hyperspectral object by a linear spectral unmixing model, which reduces the number of pixels to be recovered. Because the number of known parameters is far greater than the number of unknowns, the method enjoys an enhanced capability of successful reconstruction. We simultaneously reconstruct the true object, estimate the blurring kernels, and separate the object into spectrally homogeneous segments, each characterized by its support and spectral signature, an important step for analyzing the material compositions of space objects.

1 Introduction

The Space Situation Awareness (SSA) program functions largely in tracking, characterizing, and identifying space objects. For these purposes, ground-based imaging technologies have become indispensable tools. For acquiring useful images there has been extensive work on imaging through turbulence [1], adaptive optics (AO), e.g. [2], and image restoration techniques, e.g. [3]. But even with AO corrections, the compensation is rarely complete and image restoration techniques are often required for high resolution imagery. Among these techniques, blind deconvolution methods are often applied to jointly estimate both an object and a blurring kernel. Given the random nature of atmospheric turbulence we do not know exactly the blurring kernel to an observed image a priori, except some of the statistics of the phase function, its covariance function [1, 3, 4]. Unless the true image and the blurring kernel are parameterized with a relatively small number of parameters, the blind deconvolution problem is under-determined, i.e. the number of knowns is less than the number of unknowns. To alleviate this situation by increasing the number of observations, we can acquire multiple frames of the same object but each with a different blurring kernel before applying a blind deconvolution algorithm. This is called multiframe blind deconvolution (MFBD) [3, 5, 6, 7]. To simulatenously increase observations and reduce the number of unknowns, the phase diversity (PD) approach [8] further blurs images by adding a known phase-diversity function, usually an out-of-focus blur, to a fixed phase function, and hence multiple blurred images share not only the same object but also the same phase function. Using these images, one can set up an optimization problem to recover both the object and the phase.

So far most of the images acquired by ground-based telescopes remain monochromatic, although there have been a few studies on multispectral images, see, e.g. [9, 10, 11]. In another field of remote sensing, aerial imaging often acquires hyperspectral images spanning hundreds of bands of wavelengths by imagers looking down, in contrast to ground-based telescopes looking up. Hyperspectral images have been known to identify and unmix surface material constituents [12], and hence these images can help us characterize space objects by separating each object into different components each with a unique spectral signature, see e.g. [13].

Hyperspectral images acquired by ground-based telescopes require us estimate the PSF at each wavelength, or to blindly deconvolve and restore the true image at each wavelength, which is not only largely underdetermined, but also can be computationally prohibitive. However, as we will show in the following section, the blurring kernels across all wavelengths can be parameterized in such a way that they all share the same optimal path difference (OPD)

function [10]. In addition, we also parameterize the true object in a segmented form in which images across all wavelengths share the same support functions in the two spatial dimensions. These two parameterizations together greatly reduce the number of unknowns in the reconstruction problem. We also combine the parameterizations with the phase diversity approach by acquiring diversified images to enhance the capability of successful reconstruction, because the success of blind deconvolution large relies on coupling more observations with fewer unknowns, along with prior information.

In this paper, we discuss an optimization problem for blind deblurring hyperspectral images with only a relatively small number of parameters to estimate. The paper is organized in the following way. In Sec. 2, we describe the mathematical model of the problem and the estimation scheme, which will be followed, in Sec. 3, by image restoration results using simulated binary star images, and we conclude with discussions in Sec. 4.

2 Joint Blind Deconvolution and Spectral Unmixing

The observed, k^{th} phase-diversity image at wavelength λ is given by

$$g_\lambda(x,y) = h_{\lambda,k} * f_\lambda + \epsilon_{\lambda,k}, \tag{1}$$

where h_λ is the k^{th} phase-diversified spatially-invariant blurring kernel, or point-spread function (PSF), at wavelength λ, f_λ is the true image at wavelength λ, and $\epsilon_{\lambda,k}$ is the noise. Let K be the number of phase diversities. The blurring kernel is related to the phase function, ϕ_λ, and the phase-diveristy function, θ_k, through the expression,

$$h_{\lambda k} = \left| \mathcal{F}^{-1}\left(p e^{i(\phi_\lambda + \theta_k)} \right) \right|^2, \tag{2}$$

where p is the pupil function. If imaging a target simultaneously at multiple wavelengths, we can express the wavefront phase ϕ_λ as

$$\phi_\lambda = \frac{2\pi}{\lambda} W(x,y), \tag{3}$$

where $W(x,y)$ is the optical path difference (OPD) function. Zernike polynomials [10], or the more geometrically adaptive basis such as the disk harmonic function [11], can be used as a basis to parameterize $W(x,y)$. However, both bases wouldmight require hundreds of components for a reasonable approximation of W, and a better choice of basis would be the eigenfunctions of the covariance operator of W. If W is assumed to be sampled from a second-order stationary random process with zero mean, it is charaterized by a covariance function,

$$C(x,y,u,v) = E\left\{ W(x,y) W(u,v) \right\}, \tag{4}$$

whose associated covariance operator is

$$\mathcal{C}W(x,y) = \int\int C(x,y,u,v) W(u,v) du dv. \tag{5}$$

Here $\mathcal{C}$ is compact and self-adjoint, and hence it has a sequence of eigenvalues σ_j and corresponding eigenfunctions, $\xi_j(x,y)$. We can then project $W(x,y)$ onto the set of eigenfunction basis,

$$W(x,y) = \sum_{j=1}^{M} c_j \xi_j(x,y). \tag{6}$$

Here $\xi_j(x,y)$ is the j^{th} eigenfunction of the auto-covariance operator of W, and $c_j = \langle W, \xi_j \rangle$. $\langle \cdot, \cdot \rangle$ denotes the inner product of 2D random process. Since in this case the sequence of eigenvalues often rapidly decays to zero, we only need a few eigenfunctions to form a good approximation to W.

With frames taken within the coherence time, we can have another dimension of diversity in time, where the time-dependent blurring kernel is given by

$$h_{\lambda k t} = \left| \mathcal{F}^{-1}\left(p e^{i(\phi_{\lambda t} + \theta_k)} \right) \right|^2, \tag{7}$$

and the time-dependent phase function is

$$\phi_{\lambda t} = \frac{2\pi}{\lambda} W(x + (t-1)V_x, y + (t-1)V_y), \tag{8}$$

where V_x, V_y are the dominant wind velocities in x and y, respectively. By the shift property of Fourier transform, we have

$$\phi_{\lambda t} = \frac{2\pi}{\lambda} \mathcal{F}^{-1}\left\{ e^{i2\pi(t-1)(V_x u + V_y v)} \mathcal{F}(W) \right\}, \tag{9}$$

When $t = 1$, the equation simplifies to (3). Now we have the blurring model including time, phase and wavelength diversities:

$$g_{\lambda kt} = h_{\lambda kt} * f_\lambda + \epsilon_{\lambda kt}. \tag{10}$$

In this paper, we would bypass the time diversity by setting $t = 1$, because adding more time frames would complicate the covariance operator and we will leave it to the future research.

Next, we parameterize the hyperspectral image object by assuming the solution f is composed of a finite number of segments or materials, each of which has a homogeneous value at each spectral channel. Thus, we seek a decomposed solution which can be described in a continuous form as

$$f(x, y, \lambda) = \sum_{i=1}^{m} u_i(x, y) s_i(\lambda), \tag{11}$$

wherre $u_i(x, y)$ is the i^{th} membership function, whose values can be either 0 or 1 for a hard segmentation or in the interval [0, 1] for a fuzzy segmentation, and satises the sum-to-one constraint $\sum_{i=1}^{m} u_i(x, y) = 1$. Here, $s_i(\lambda)$ represents the spectral signature of the i^{th} segment or material. The support of u_i lies only on the two spatial dimensions represented by x and y, and is thus independent of the spectral dimension represented by λ, while on the other hand, the spectral signatures, $s = \{s_i(\lambda)|i = 1, ..., m\}$, vary only along the spectral dimension. Hence, the original three-dimenstional function, $f(x, y, \lambda)$, is represented by a finite number of two-dimensional and one-dimensional functions. The discrete version of f can be written as

$$f = \sum_{i=1}^{m} u_i^T s_i, \tag{12}$$

where $f \in \mathbb{R}^{n_1 n_2 \times d}$ is the folded hyperspectral cube, $u_i \in \mathbb{R}^{n_1 n_2}$ is the vectorized membership function and $s_i \in \mathbb{R}^d$. Here d is the number of spectral channels, m is the number of segments or materials, and n_1 and n_2 are the numbers of pixels in x and y respectively. For an example of such formulation, see the Hubble Space Satellite example in [13].

Eq. (11) can be called a linear spectral-unmixing model, if $s_i(\lambda)$ is assumed to be the spectral signature of the i^{th} pure material, and $u_i(x, y)$ is the weight of the i^{th} pure pixel's contribution to the pixel at (x, y). This formulation especially suits the hyperspectral imaging of space objects, because we often expect less blurring due to atmosphere turbulence in longer wavelengths, where sharper images will provide us better estimation of wavelength-independent membership functions, which can then be used to estimate spectral signatures at shorter wavelengths.

To summarize the model, we have blurred, noisy, and spectrally-mixed images, $g_{\lambda k}$, as our observations, from which we reconstruct the true hyperspectral image object, parameterized by s and u, while simultaneously estimating the blurring kernel parameterized by the OPD function, independent from wavelengths or phase diversities, and which is further parameterized by the eigenfunctions of its covariance operator. The number of known observations, dKn_1n_2, will be far greater than the number of unknowns, $M + md + mn_1n_2$, if $dK \gg m$, and hence we expect a high probability of successful reconstruction. The model embeds a spectral-unmixing model within a blind-deconvolution phase diversity model, and thus we call it a joint blind-deconvolution and spectral-unmixing model.

3 Numerical Optimization

The optimization scheme follows largely the one by Vogel, Chan and Plemmons [4], and hence we first introduce their phase-diversity cost functional

$$J(f, \phi) = \frac{1}{2} \sum_{k=1}^{K} \int_{\mathbb{R}^2} [h_k(\phi) * f - g_k]^2 + \frac{\gamma}{2} \int_{\mathbb{R}^2} f^2 + \frac{\alpha}{2} \sum_{j=1}^{M} \frac{|c_j|^2}{\sigma_j}. \tag{13}$$

The first term on the right hand side (RHS) is the least squares term corresponding to the Gaussian noise assumption, and the second term is the Tikhonov regularization of f, while the last term is the regularization of the phase function, ϕ. Since we further parameterize f, our cost functional would be

$$J(W, u, s) = \frac{1}{2} \sum_{\lambda=1}^{d} \sum_{k=1}^{K} \int_{\mathbb{R}^2} [h_{\lambda k}(W) * \sum_{i=1}^{m} s_i(\lambda) u_i - g_{\lambda k}]^2 + \frac{\gamma}{2} \sum_{i=1}^{m} \int_{\mathbb{R}^2} u_i^2 + \frac{\alpha}{2} \sum_{j=1}^{M} \frac{|c_j|^2}{\sigma_j}. \tag{14}$$

Comparing (13) and (14), we can see that in (14), there is an extra wavelength diversity in the least squares term,

We take the alternating approach to estimate four sets of parameters, i.e., at the i^{th} iteration,

1. given the current estimates, $\hat{W}^{(i-1)}, \hat{u}^{(i-1)}$, we solve for the spectral signatures, $\hat{s}^{(i)}$;
2. given the current estimates, $\hat{W}^{(i-1)}, \hat{s}^{(i)}$, we solve for the membership functions, $\hat{u}^{(i)}$;
3. given the current estimates, $\hat{u}^{(i)}, \hat{s}^{(i)}$, we solve for $\hat{W}^{(i)}$.

Next, we explain each step in detail.

3.1 Estimate spectral signatures

In the first step, if $m = 1$, meaning that there is only a single segment/material in the scene, we can solve for its spectral response, $s(\lambda)$, without the need of knowing the PSF, $h_{\lambda k}$. Choose one k in the set, $\{1, \ldots, K\}$, and let $H_{\lambda k} = \mathcal{F}(h_{\lambda k})$. We know $\tilde{H}_{\lambda k}(1,1) = 1$, since the integral of the PSF is always 1. With a known support function u, we have

$$s(\lambda) = \frac{G_{\lambda k}(1,1)}{U(1,1)}, \tag{15}$$

where $G_{\lambda k} = \mathcal{F}(g_{\lambda k})$ and $U = \mathcal{F}(u)$. This approach is especially useful in imaging a single star and estimating its spectral signatures without estimating the wavelength-dependent PSFs, see, e.g., the MUSE system in [14]. If $m > 1$, meaning that there are more than one segment/material in the scene, we can also solve for their approximate spectral response at other wavelengths, $s_i(\lambda)$, through choosing a small neighborhood of $\tilde{H}_{\lambda k}(1,1)$ to set up a linear equation set. For example if $m = 4$, we can construct a 4×4 matrix A, the i^{th} row of which is

$$A_i = [H_{\lambda,k}(1,1)U_i(1,1), H_{\lambda,k}(1,2)U_i(1,2), H_{\lambda,k}(2,1)U_i(2,1), H_{\lambda,k}(2,2)U_i(2,2)], \tag{16}$$

and construct a column vector,

$$b = [G_{\lambda k}(1,1); G_{\lambda k}(1,2); G_{\lambda k}(2,1); G_{\lambda k}(2,2)], \tag{17}$$

and the solution would be

$$s_\lambda = A^{-1}b. \tag{18}$$

Because we only use the low-frequency parts of $h_{\lambda,k}$, which are often better estimated than the high-frequency parts, we would have a better estimate for s_λ by removing the high-frequency parts in its estimation.

3.2 Estimate membership functions

With known phase functions and spectral signatures, the cost functional (14) simplifies to a least-squares inverse problem. Here we stabilize the computations with Tikhonov regularization. We First take the Fourier transform of the least square term and denote $b_{\lambda,k}(s,t) = G_{\lambda k}(s,t)/H_{\lambda k}(s,t)$. We group all $b_{\lambda,k}(s,t)$ into a single column vector, $b_{st} \in \mathbb{R}^{dK}$, and for each (s,t), group all $\{U_i(s,t) = |i = 1, \ldots, m\}$ into a column vector, $\tilde{u}_{st} \in \mathbb{R}^m$. After some manipulations, we have the following simplified functional,

$$\|A\tilde{u}_{st} - b_{st}\|_2^2 + \frac{\gamma}{2}\|\tilde{u}_{st}\|_2, \tag{19}$$

where $A = S \otimes \mathbf{1}$, S is a matrix whose i^{th} column is s_i, and $\mathbf{1} \in \mathbb{R}^K$ is a constant vector of ones. We solve the functional above for each (s,t), and group them back in U_i and hence $u_i = \mathcal{F}^{-1}(U_i)$.

3.3 Estimate phase functions

With known spectral signatures and membership functions, the cost functional reduces to (13), and like [4], we use the Newton method to update W, i.e.,

$$W^{i+1} = W^i - H[W^i]g[W^i], \tag{20}$$

where $H[W^i]$ is the Hessian matrix of $J(W^i)$ at the i^{th} iteration, and $g[W^i]$ is the gradient of $J(W^i)$. An explicit form of the gradient of $J(\phi)$ is provided in [4], which only differs from $J(W)$ by a constant $2\pi/\lambda$, and the computation codes in MATLAB are provided by Bardsley [15].

The Hessian matrix is approximated by the limited-memory Broyden-Fletcher-Goldfarb-Shanno (L-BFGS) method [16]. The original BFGS method approximates the Hessian matrix using rank-one updates specified by gradient evaluation, and unlike the original BFGS method which stores a dense approximation, L-BFGS stores only a few vectors that represent the approximation implicitly. Considering the Hessian matrix has size $n_1n_2 \times n_1n_2$, we believe the limited-memory approximation is appropriate.

4 Numerical Results

We simulate a set of observed hyperspectral images of a binary star, for which the true hyperspectral data is zero everywhere except at two pixels, each of which has a different spectral signature taken from a NASA material library sent to us by Kira Abercromby. We simulate a von Karman phase spectrum as

$$P(x,y) = \sqrt{.023}(D/r_0)^{5/6}(x^2+y^2)^{-11/6}, \tag{21}$$

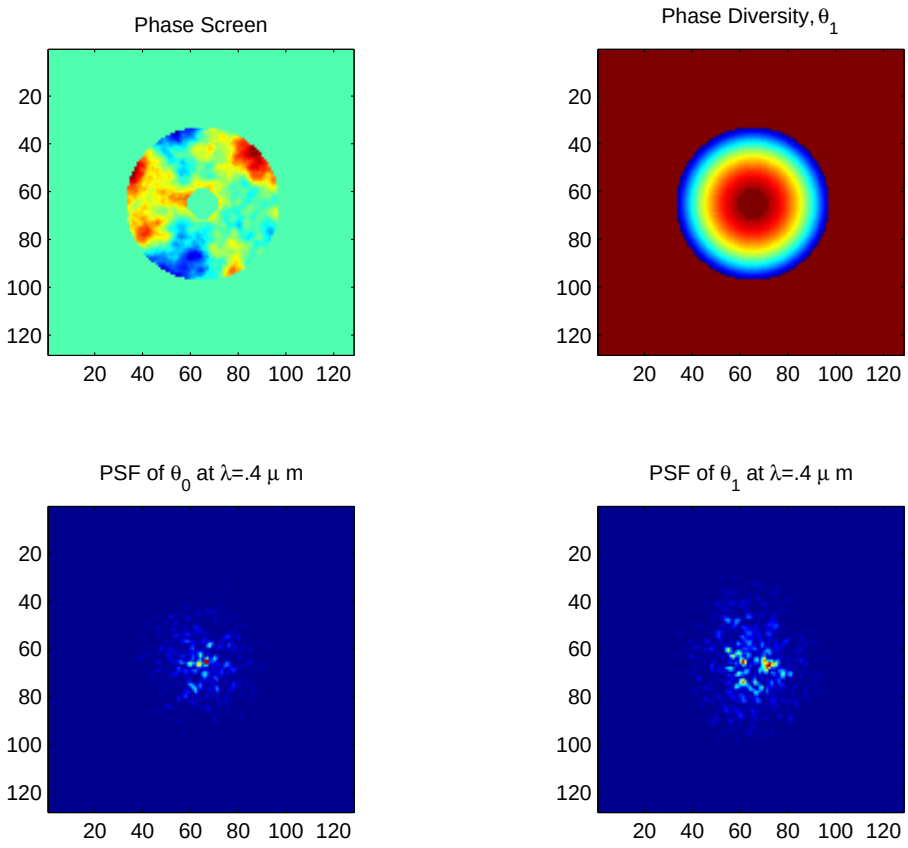

Figure 1: Phase, phase diversity and corresponding PSFs.

where D is the aperture diameter, and r_0 is Fried parameter. Here, we fix D/r_0 at 10. The phase screen or the OPD function, is then generated by multiplying $P(x, y)$ with standard noise as

$$W(x, y) = P(x, y)\xi(x, y), \tag{22}$$

where $\xi(x, y)$ is complex standard white noise. Hence, $P(x, y)$ is the diagonal covariance function of $W(x, y)$, meaing that $W(x_1, y_1)$ is independent from $W(x_2, y_2)$ for $\forall x_1 \neq x_2$ and $\forall y_1 \neq y_2$. In the regularization term of the cost functional, we use $\sqrt{P(x, y)}$ as $\sigma_j(x, y)$ in (14), which is equivalent to setting M as 1. Corresponding to a telescope with a large circular primary mirror with a small secondary mirror at its center, the pupil function is taken to be the indicator function of an annulus. For the phase diversity function, we set $\theta_1(x, y) = cp(x^2 + y^2)$, where c is a constant and p is the pupil function. The spatial domain is a 128×128 pixel array. The simulated phase, phase diversity and a couple PSFs are shown in Figure 1.

We then convolve the PSFs, $h_{\lambda k}$, with the hyperspectral image cube of a simulated binary star to simulate twenty blurred images with added white noise, shown in Fig. 2. Clearly, images at lower wavelengths suffer more from stronger blurring, while images at longer wavelengths are much more clear. This justifies our idea that the spectral-independent membership functions, u, derived from longer wavelengths can used for spectral signature reconstruction in the longer wavelengths. Note that we have not considered the diffraction effects here for longer wavelength, because our longest wavelength is $2.4\mu m$.

Figure 3 compares the estimated OPD function with the true one, and clearly the estimate is close to the true OPD except in some high frequency parts. Figure 4(a) presents the estimated spectral signatures in blue compared with the true ones in red, which are both quite similar in shape, though off by a certain scale. Note that usually it is hard to estimate spectral responses at lower wavelengths without using the approach in (18), and for comparison,

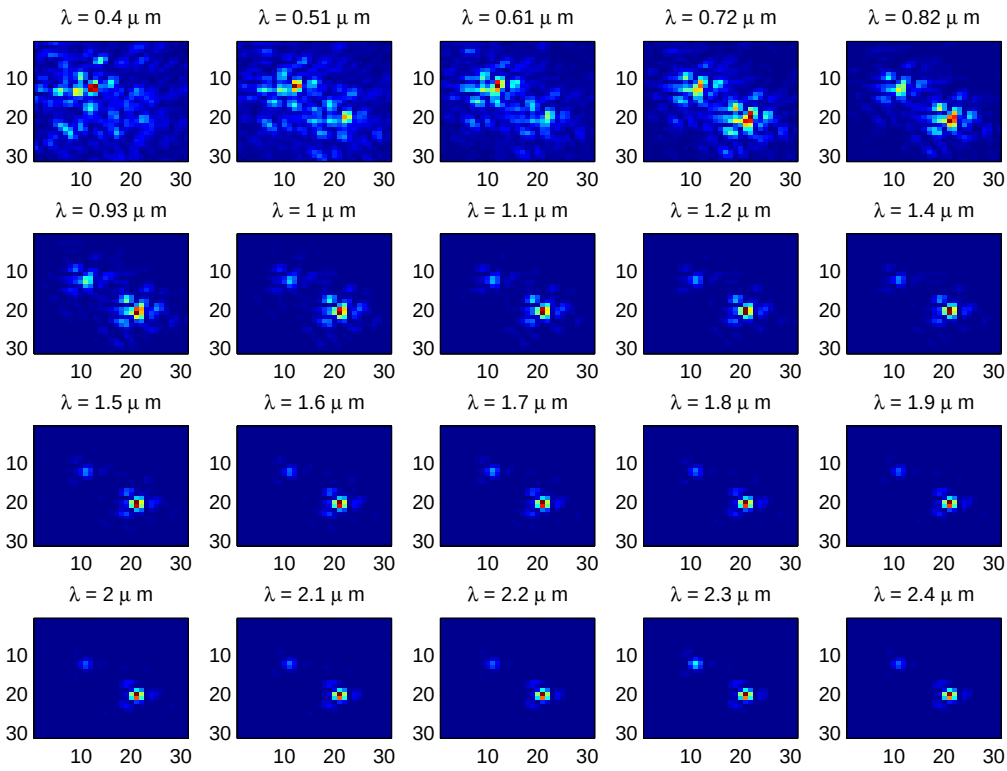

Figure 2: Simulated hyperspectral images with $\theta_1 = c(x^2 + y^2)$.

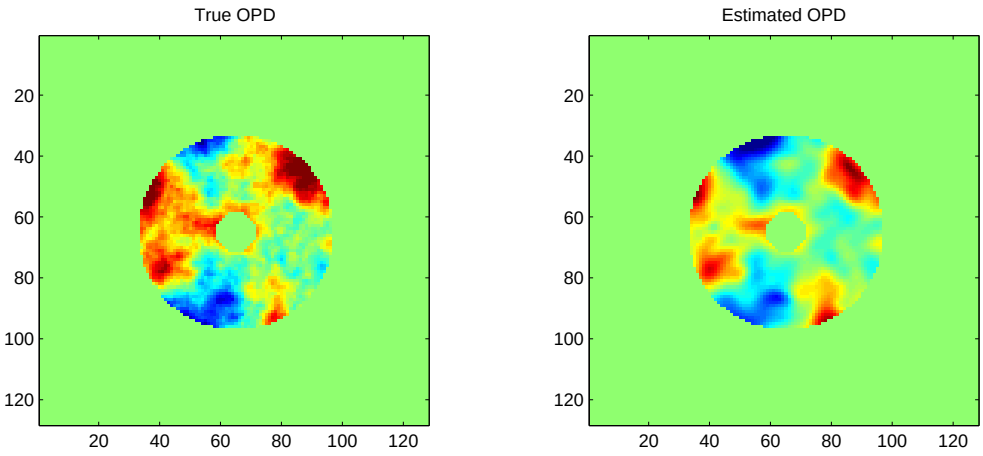

Figure 3: Comparison of the true OPD function with the estimated OPD function.

we also show the signatures extracted from an esimate of f without the segmented solution form in Fig. 4(b), and clearly, we see the poorer estimates across all wavelengths.

Figure 5 shows the zoomed-in membership functions, where u_1 is the membership function of the star on the top left, and u_2 is the membership function of the star on the bottom right. The sharp contrasts around the brightest pixels in u_1 and u_2 demonstrate the good quality of estimates.

5 Conclusions

We have presented a joint model of blind-deconvolution and spectral-unmixing for reconstructing true image objects and estimating blurring kernels from blurred and noisy hyperspectral images of space objects. An alternating optimization scheme is presented for jointly estimating spectral signatures and membership functions of space object components, along with the blurring kernels parameterized by the optical path function. The model enjoys a much smaller set of parameters when compared to the MFBD approach while wavelength diversity plus the phase diversity increases the number of observed images of the same astronomical objects. We feel that more observations combined with fewer parameters can enhance reconstruction success.

Acknowledgements

Research by R. Plemmons and Q. Zhang is supported by the U.S. Air Force Office of Scientific Research (AFOSR), under Grant FA9550-11-1-0194.

References

[1] M. C. Roggemann and B. M. Welsh, *Imaging through turbulence*. CRC press, 1996.

[2] F. Roddier, *Adaptive Optics in Astronomy*. Cambridge university press, 1999.

[3] C. L. Matson, K. Borelli, S. Jefferies, C. C. Beckner Jr, E. K. Hege, M. Lloyd-Hart, *et al.*, "Fast and optimal multiframe blind deconvolution algorithm for high-resolution ground-based imaging of space objects," *Applied Optics*, vol. 48, no. 1, pp. A75–A92, 2009.

[4] C. R. Vogel, T. F. Chan, and R. J. Plemmons, "Fast algorithms for phase-diversity-based blind deconvolution," in *Astronomical Telescopes & Instrumentation*, pp. 994–1005, International Society for Optics and Photonics, 1998.

[5] T. J. Schulz, "Multiframe blind deconvolution of astronomical images," *JOSA A*, vol. 10, no. 5, pp. 1064–1073, 1993.

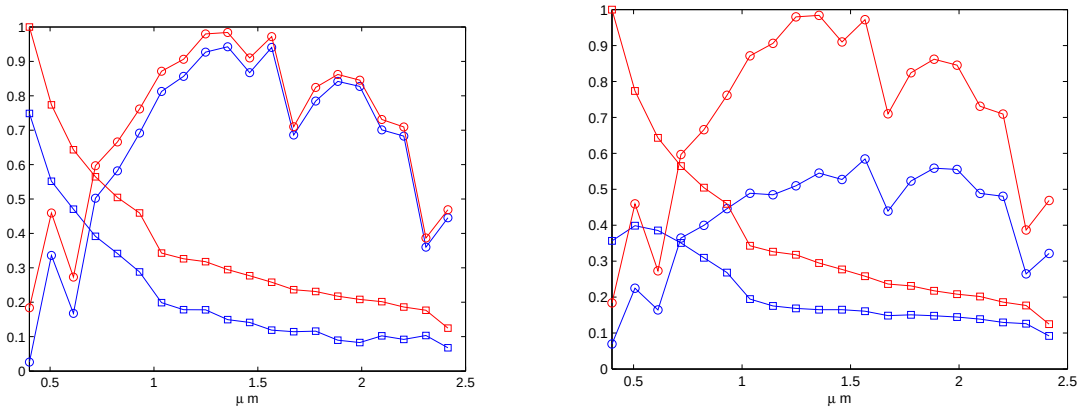

(a) (b)

Figure 4: (a) Comparison of the estimated spectral signatures in blue with the true signatures in red. (b) Estimated signatures without the segmented form of solution.

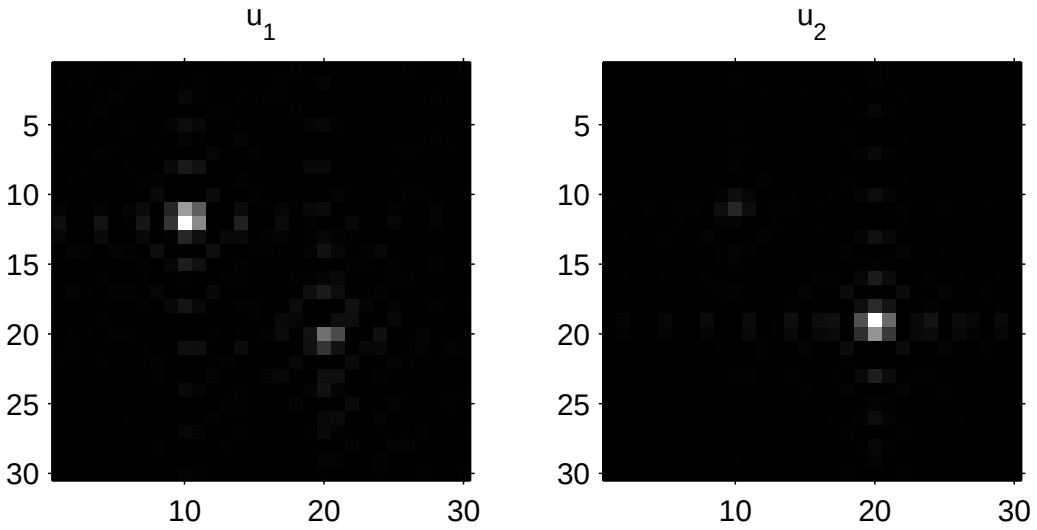

Figure 5: Estimated membership functions, $u_i, i = 1, 2$.

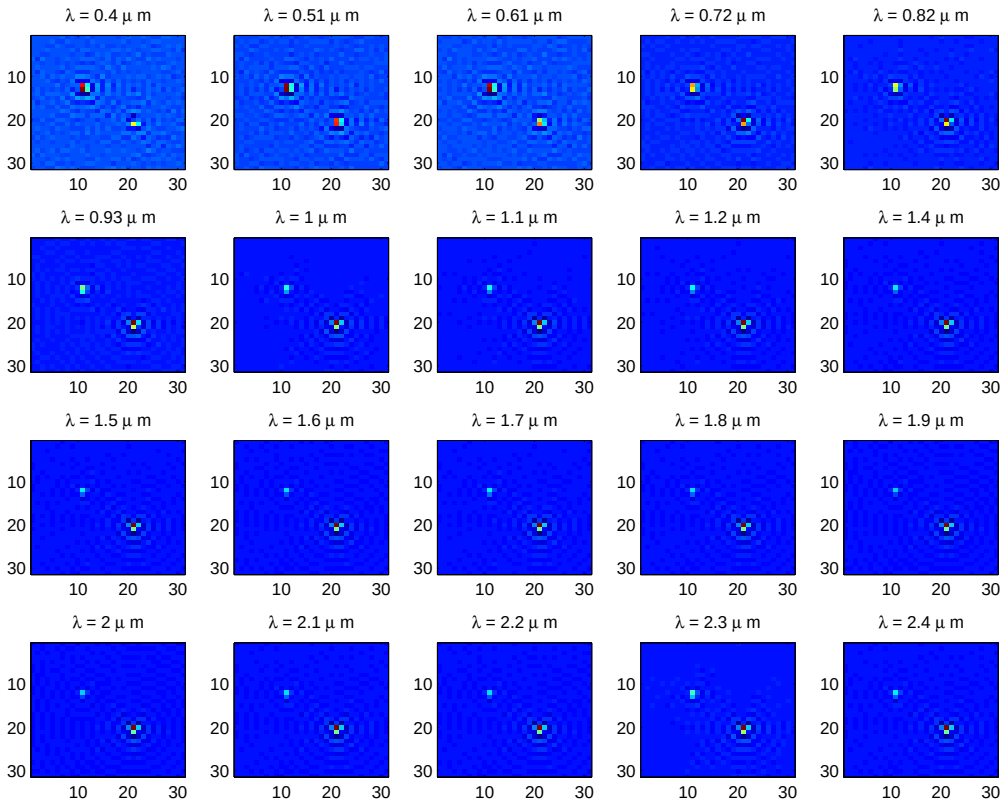

Figure 6: Estimated hyperspectral images, $f(x, y, \lambda)$, in twenty spectral channels.

[6] D. A. Hope and S. M. Jefferies, "Compact multiframe blind deconvolution," *Optics Letters*, vol. 36, no. 6, pp. 867–869, 2011.

[7] S. M. Jefferies and M. Hart, "Deconvolution from wave front sensing using the frozen flow hypothesis," *Optics express*, vol. 19, no. 3, pp. 1975–1984, 2011.

[8] R. A. Gonsalves, "Phase retrieval and diversity in adaptive optics," *Optical Engineering*, vol. 21, no. 5, pp. 215829–215829, 1982.

[9] T. F. Blake, M. E. Goda, S. C. Cain, and K. J. Jerkatis, "Enhancing the resolution of spectral images," in *Defense and Security Symposium*, pp. 623309–623309, International Society for Optics and Photonics, 2006.

[10] D. A. Hope, S. M. Jefferies, and C. Giebink, "Imaging geo-synchronous satellites with the AEOS telescope," in *Advanced Maui Optical and Space Surveillance Technologies Conference*, vol. 1, p. 33, 2008.

[11] S. M. Jefferies, D. A. Hope, and C. Giebink, "Next generation image restoration for space situational awareness," tech. rep., DTIC Document, 2009.

[12] M. T. Eismann, *Hyperspectral Remote Sensing*. SPIE Press, 2012.

[13] Q. Zhang, H. Wang, R. Plemmons, and V. Pauca, "Tensor methods for hyperspectral data analysis: a space object material identification study," *Journal of the Optical Society of America A*, vol. 25, no. 12, pp. 3001–3012, 2008.

[14] D. Serre, E. Villeneuve, H. Carfantan, L. Jolissaint, V. Mazet, S. Bourguignon, and A. Jarno, "Modeling the spatial PSF at the VLT focal plane for MUSE wfm data analysis purpose," in *SPIE Astronomical Telescopes and Instrumentation: Observational Frontiers of Astronomy for the New Decade*, pp. 773649–773649, International Society for Optics and Photonics, 2010.

[15] J. Bardsley, S. Jeffries, J. Nagy, and R. Plemmons, "A computational method for the restoration of images with an unknown, spatially-varying blur," *Optics Express*, vol. 14, no. 5, pp. 1767–1782, 2006.

[16] J. Nocedal, "Updating quasi-newton matrices with limited storage," *Mathematics of computation*, vol. 35, no. 151, pp. 773–782, 1980.